J. Fluid Mech. (1989), *vol.* 204, *pp.* 1–30
Printed in Great Britain

Scaling of hard thermal turbulence in Rayleigh–Bénard convection

By BERNARD CASTAING†, GEMUNU GUNARATNE‡, FRANÇOIS HESLOT§, LEO KADANOFF‡, ALBERT LIBCHABER‡, STEFAN THOMAE‖, XIAO-ZHONG WU‡, STÉPHANE ZALESKI¶ AND GIANLUIGI ZANETTI‡

† CNRS-CRTBT, 25 Avenue des Martyrs-P.B. 166X, 38042 Grenoble Cedex, France

‡ The Research Institutes, The University of Chicago, 5640 S. Ellis Avenue, Chicago, IL 60637, USA

§ Collège de France, Matiere Condensée, Place Marcellin Berthelot, 75005 Paris, France

‖ Institut für Festkörperforschung der KFA, Postfach 1913, D-5170 Jülich, W. Germany

¶ Laboratoire de Physique Statistique, ENS, 24 rue Lhomond, 75231 Paris Cedex 05, France

(Received 24 February 1988 and in revised form 30 August 1988)

An experimental study of Rayleigh–Bénard convection in helium gas at roughly 5 K is performed in a cell with aspect ratio 1. Data are analysed in a 'hard turbulence' region ($4 \times 10^7 < Ra < 6 \times 10^{12}$) in which the Prandtl number remains between 0.65 and 1.5. The main observation is a simple scaling behaviour over this entire range of Ra. However the results are not the same as in previous theories. For example, a classical result gives the dimensionless heat flux, Nu, proportional to $Ra^{\frac{1}{3}}$ while experiment gives an index much closer to $\frac{2}{7}$. A new scaling theory is described. This new approach suggests scaling indices very close to the observed ones. The new approach is based upon the assumption that the boundary layer remains in existence even though its Rayleigh number is considerably greater than unity and is, in fact, diverging. A stability analysis of the boundary layer is performed which indicates that the boundary layer may be stabilized by the interaction of buoyancy driven effects and a fluctuating wind.

1. Introduction

In this paper we describe some results on a particular regime of turbulence observed in thermal convection. The main objective of the paper is to propose a phenomenological explanation of those results. Thermal convection is a subject of longstanding interest and has many applications in science and engineering. Solar and stellar structure is greatly dependent on how heat is transported from the core to the exterior; heat transport in the Earth's mantle is also of paramount importance to geophysics. Heat transport problems are also frequently encountered in technological applications. Our study of thermal convection is however motivated by basic science. This system is in many respects of unsurpassed simplicity for the study of the irregular and complex motions in fluids and hence is well-suited for a fundamental study. It has an advantage over open flow systems because of the greater ease with which very well-defined boundary conditions can be realized experimentally. In a cavity one only needs to control the temperature of the walls and this can be done to a remarkable precision and with great stability over a long period of time. In open flows, it is hard to make a well-specified and reproducible flow

at the inlet. On the theoretical level the simplicity of the fundamental convective state is also of great help. For all those reasons much interesting work on nonlinear problems was done on convective systems. Malkus & Veronis (1958) showed how the nonlinear analysis of the Bénard instability could be performed. The various stability properties of the nonlinear convective state were studied in detail and reviewed by Busse (1978). In a different spirit modern approaches on dynamical systems were initiated by the study of thermal convection by Lorenz (1963). Many experiments on chaotic dynamics were performed on convective systems (for example Libchaber & Maurer 1982) near the onset of chaos.

More recently, we set up a convective experiment in which we could sweep the whole range from conduction to turbulent behaviour. Our experiment involves convective flow in helium gas (see Threlfall 1975) at low temperatures, about 5 °K. Preliminary results and some interpretation were published in a previous paper (Heslot, Castaing & Libchaber 1987). This paper suggests a classification of the different regimes that were observed depending on the Rayleigh number

$$Ra = \frac{\alpha g \Delta L^3}{\kappa \nu}. \tag{1.1}$$

Here g is the acceleration due to gravity, α is the volume thermal expansion coefficient, Δ is the temperature difference between the bottom and top of the cell and κ and ν are respectively the thermal diffusivity and kinematic viscosity.

Most of the preceding studies describe the fluid as turbulent as soon as the behaviour is non-periodic. Recently (Heslot *et al.* 1987; Eckmann 1981) it became obvious however that the first non-periodic behaviour (called here chaos) is very different from developed turbulence. The difference is that in the chaotic state only the time coherence is lost while the space coherence persists. The chaotic system is always fully spatially coherent. In the same spirit one can expect to have to distinguish between different types of turbulence. Heslot *et al.* (1987) outlined the classification we employ: after chaos a transition regime where the coherence between the probes is lost, then two turbulent states which we call soft and hard turbulence. To justify this classification and characterize these states Heslot *et al.* used the classical statistical tools: power spectra, cross correlations between the two local probes and histograms of temperature fluctuations.

In this paper, we focus our attention upon the larger scale properties of the turbulent behaviour in the previously identified hard-turbulence regime. Our particular goal is to pick out some of the simple-scaling behaviour exhibited in the data and to describe this behaviour via a kind of scaling or similarity theory.

1.1. *Previous theories and experiments*

The high-Rayleigh-number regime of convective flow has been investigated extensively. Both experimental and theoretical studies abound. Over 400 references may be found (Behringer 1985; Busse 1978; Koschmieder 1974). Here we first present some of the most discussed predictions of theory and then assess the experimental evidence existing in the literature. A summary is given in table 1. Two kinds of idealized geometries are often investigated: a hot plate with an infinitely extended medium on top of it and a layer with horizontal top and bottom plates and a very large Rayleigh number. The first situation was investigated by Prandtl (1932). In a steady state regime the heat flux H must be fixed throughout the layer. If the typical velocity and temperature scales at a height z above the plate are $u(z)$ and $T(z)$

respectively, one obtains, neglecting the contribution of conduction to the heat flux,

$$H \sim u(z)\, T(z). \tag{1.2}$$

In all the following reviews and in the exposition of the new theory we shall not try to estimate dimensionless constants of order unity and leave the results in the above form. The free fall velocity over height z is

$$u(z) \sim (g\alpha T(z)\, z)^{\frac{1}{2}}, \tag{1.3}$$

as a result

$$g\alpha T(z) \sim (H^2 g^2 \alpha^2)^{\frac{1}{5}} z^{-\frac{1}{3}}. \tag{1.4}$$

This result can also be obtained through dimensional analysis. This is the only power law in which the molecular transport coefficients κ and ν do not appear and it is hence the only appropriate law in the limit of high Rayleigh number.

Prandtl's 'free fall' similarity theory does not however specify the heat flux in a layer of finite height. Another kind of similarity argument is needed. It is applicable to layers at high Rayleigh number (Howard 1963). A high Rayleigh number can be obtained by fixing temperature on both plates but letting the height L grow indefinitely. If a regime independent of the height of the box develops near the bottom plate the heat flux should reach a finite limit independent of the height of the box. The only power law that satisfies this requirement is (Priestley 1954)

$$Nu \sim Ra^{\frac{1}{3}}, \tag{1.5}$$

where Nu is the ratio of the total heat flux to the conductive heat flux

$$Nu = HL/\kappa \Delta. \tag{1.6}$$

The free fall assumption and this classical $\frac{1}{3}$ law are actually relatively independent assumptions. Both are obtained through assumptions about the limit of infinite Rayleigh number. In a finite box however the free fall theory is best viewed as a particular assumption about the behaviour in the interior of the flow. The $\frac{1}{3}$ law is rather an assumption about boundary layers. In the free fall theory the interior can reach a regime of $Nu \sim Ra^{\frac{1}{2}}$ and is hence quite inefficient in limiting the heat flux. It is hence plausible that the heat flux is determined by the boundary layers.

More detailed investigations of both the interior and boundary layer classical similarity theories abound. Monin & Obukhov (1953, 1954, see also Monin & Yaglom 1971, chapter 7 and the references they cite) investigated thermally stratified shear layers with a horizontal wind. Priestley (1959) gave a detailed description of the atmospheric boundary layer using various similarity hypotheses.

The experiments and theory of Malkus (1954*a*, *b*, 1963) gave an analysis of the turbulent regime in terms of marginal stability of the mean flow and other related assumptions (see also the interesting reformulation of the theory by Spiegel 1962). This approach allows one to derive the $\frac{1}{3}$ law without reference to similarity theory, and gives a temperature dependence in the interior that seems in better agreement with experiment.

The idea that the boundary layer is marginally stable is a crucial point in the theory presented by Malkus (1954*b*, 1963) but has been further developed in Howard's work. His argument (Howard 1966) is as follows: if there is a thermal boundary layer of width λ above which the temperature gradient is negligible and below which there is no fluid motion the heat flux is given by

$$H \sim \kappa \Delta/\lambda. \tag{1.7}$$

Quantity	Amplitude Experiment	Name	Index Experimental value	Theoretical values Present paper	Classical
Nu	0.23 ± 0.03	β	0.282 ± 0.006	$\frac{2}{7}$	$\frac{1}{3}$
Δ_c/Δ	0.36 ± 0.04	γ	-0.147 ± 0.005	$-\frac{1}{7}$	$-\frac{1}{9}$
$\omega_p L^2/\kappa$	0.36 ± 0.01	δ	0.491 ± 0.002	$\frac{1}{2}$	$\frac{2}{3}$
$u_c L/\nu$	$1.05\,Pr^{-\frac{2}{3}}$	ϵ	0.43	$\frac{3}{7}$	$\frac{4}{9}$
$\langle T(z)\rangle/\Delta$	varies	s	varies	0	$\frac{1}{3}$

TABLE 1. Summary of index values. The origin of the data and the theoretical predictions are given in the text. The fits are all in the form quantity = Amplitude $\times Ra^{\text{index}}$ except for the temperature which scales as a power of the distance from the bottom plate (see also §1.2).

The width λ must be small enough so that the layer is stable but will tend to grow by diffusion. The stability of the layer is determined by its Rayleigh number

$$Ra^{\text{bl}} = \frac{\alpha g \Delta \lambda^3}{\kappa \nu}. \tag{1.8}$$

The value for instability can be extrapolated (Chandrasekhar 1961) from known results for simple layers (Pellew & Southwell 1940; Reid & Harris 1958) and a reasonable value is $Ra_c \approx 10^3$. One obtains

$$Nu \approx (Ra/Ra_c)^{\frac{1}{3}}. \tag{1.9}$$

The coefficient and index of that law have been considered in good agreement (within 10%) with experiments at moderate Rayleigh numbers.

Other theories in the spirit of Malkus' and Howard's theory have been developed by several authors. Herring (1963, 1964), Roberts (1966), Gough, Spiegel & Toomre (1975) and Toomre, Gough & Spiegel (1977, 1982) developed so called 'mean field theories' where several modes are considered on top of the marginally stable mean temperature field conjectured by Malkus. The optimum theories of Howard (1963), Busse (1969, 1978*b*) and Chan (1971) attempt to find an upper bound on turbulent heat transport. This upper bound is expected to be realized if the heat flux is optimal with respect to the constraints stated in the theory.

Kraichnan (1962) refined the similarity theory to include a double boundary layer. One of the interesting results of his analysis is that a modification of the classical scaling (1.9) is to be expected around $Ra = 10^{18}$ because of the interaction of the boundary layer with a horizontal fluctuating wind. Our work, which builds upon Kraichnan's is also a similarity theory. The advantage of working with such similarity theories is that many predictions are made easily from dimensional analysis. On the other hand the choice of the lengthscales that are introduced, and those which are not considered, may seem somewhat arbitrary. Experiments provide a check on whether the similarity theory grasps the relevant phenomena.

1.2. *Outline of the paper*

The next section of the paper describes the experiment and compares them with the predictions of the classical boundary-layer theory, which is found to be inconsistent with the data. Another similarity theory is developed in §3 and the various scaling indices thus obtained are compared with experiment. A more detailed theoretical

description of how the classical description of the boundary layer breaks down in the presence of turbulence in the interior is presented in §4. For the sake of the reader who would desire a quick look at the results without entering the detailed exposition we show the major scaling results of the new theory in table 1. In this table we give the observed experimental power laws and also give our theoretical predictions for the indices. For comparison some classical values of the indices are also provided. We use free fall theory for the velocity estimate. The quantities in the table are

(i) The dimensionless heat flux Nu.

(ii) A typical observed value of the temperature fluctuation near the centre of the cell Δ_c. Its precise definition is given in §2.

(iii) A resonant frequency ω_p observed near the bottom of the cell. The frequency of boundary layer detachments predicted by Howard (1966) is chosen as a classical value although the mechanism of this pulsation might be entirely different.

(iv) An interesting result not drawn from our experiment is the measurement of the typical velocity in the interior by Tanaka & Miyata (1980). The free fall theory ($s = \frac{1}{3}$) was used to predict the index for the speed in the 'theoretical' value column.

(v) The observed temperature decay away from the boundary layer measured in terms of the boundary-layer width, that is $\langle T(z)\rangle/\Delta \approx (z/\lambda)^{-s}$. In our theory there is no steep variation of the typical temperature as the fluid rises in the interior. This is expressed in equation (3.12).

In the work described below, Bernard Castaing, François Heslot, Albert Libchaber and Xiao-Zhong Wu were primarily responsible for the experiment. Primary responsibility for data transfer and analysis fell to Gemunu Gunaratne, Stefan Thomae and Gianluigi Zanetti, primary responsibility for the scaling theory lies with Leo Kadanoff, Stéphane Zaleski and Gianluigi Zanetti and the stability theory belongs to Stéphane Zaleski.

2. The experiment

2.1. *Experimental set-up and procedure*

As was noted by Threlfall, gaseous ^{4}He at low temperature (5 °K) is an interesting fluid. The Rayleigh number can be easily controlled since in the dilute gas regime, both ν and κ are inversely proportional to the density. Moreover the pressure of the critical point of ^{4}He is reasonably low: 2.2 atm. One can thus vary the coefficient in front of Δ in equation (1.1) over a very wide range. On the other hand the Prandtl number, $Pr = \nu/\kappa$, remains between 0.65 and 1.1 up to $Ra = 10^{11}$ and then increases up to 1.5 for $Ra = 10^{12}$. The Prandtl number increases further in the neighbourhood of the critical point. To eliminate the effect of this rise, we do not include data for $Ra > 10^{12}$ in our analysis.

Other advantages of the low temperature environment are the sensitivity and short response time of the probes. The sensitivity is due to the low thermal noise and the rapid variation of the resistance of the probes with the temperature

$$\frac{\mathrm{d}r}{r} \approx 2\frac{\mathrm{d}T}{T}.$$

The usual counterpart, that is the $1/f$ noise, is very small in our Si bolometers and not visible in our range of frequencies. The short response time is due to the low specific heat of Si at this temperature. On the other hand, the electron–phonon

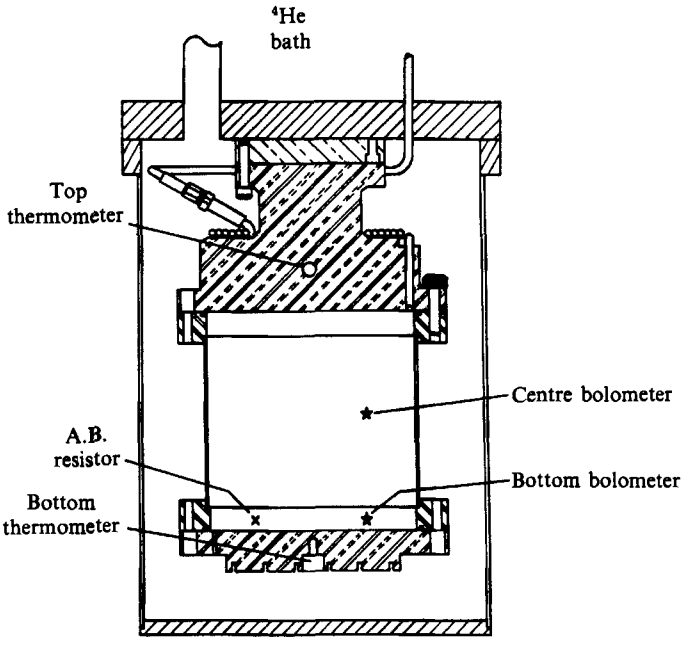

FIGURE 1. The experimental set-up.

decoupling could be a problem only at lower temperature. We have measured the response time to a self heating to be less than 1 ms, well beyond our needs.

Let us now describe the cell (see figure 1). It has the shape of a vertical cylinder whose diameter is equal to its height: $L = 8.7$ cm. The aspect ratio is thus 1. The thin stainless steel wall of the cell is thermally isolated from the main liquid helium bath by a vacuum jacket. The gas filling tube has a 2 m long thermalization on the upper plate before entering the cell and can be closed near the cell in the helium bath. The upper plate is thermally regulated by a linear research LR-130 regulation system. The bottom plate is heated with constant d.c. power using a four-wire method for the precise measurement of power. Both plates are made of thick pure copper with calibrated Ge thermometers in each. Two local arsenic-doped silicon far-infrared detectors, 200 μm in size are used to measure local temperature fluctuations. The 'bottom' one is placed above the bottom plate and inside the cell, half a radius in distance from the cell axis and 200 μm from the bottom plate. The centre bolometer is placed right above the bottom one at equal distances from both plates. An Allen Bradley resistance, thinned down in size is placed 5 mm above the bottom plate as shown in figure 1.

The sensors as well as the Ge thermometers of the plates are measured using a four-wire bridge of the type described by Anderson (1973). Measured in the usual way, avoiding self heating by the testing current, they provide the local temperature fluctuations of the fluid. On the other hand, with a strong measuring current their temperature is no longer characteristic of the local temperature, but of the local velocity, on which the cooling rate is dependent. This is the well-known hot-wire technique, widely used in aerodynamics.

The signal of each bridge is measured by a PAR lock-in amplifier. The outputs of these lock-in amplifiers can be sent to a multiprogrammer HP6942A for digital

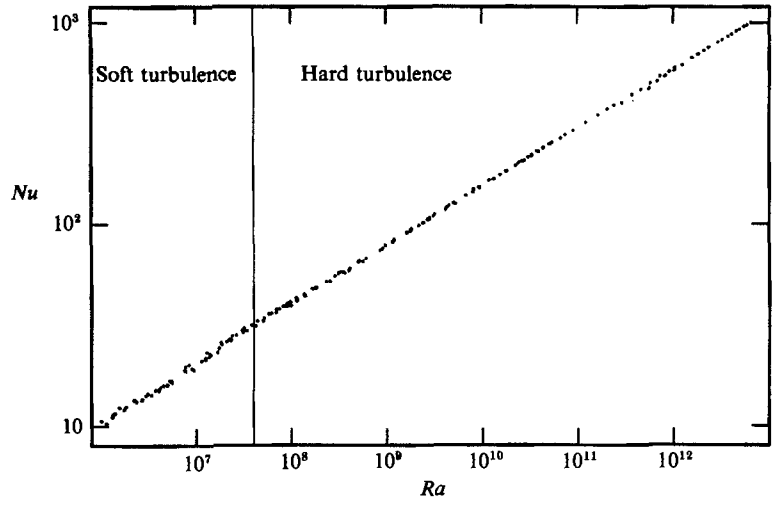

FIGURE 2. The *Nu–Ra* correlation. The vertical line at $Ra = 4 \times 10^7$ indicates the transition from soft to hard turbulence.

acquisition, or to a HP3562A Digital Signal Analyzer for statistical treatment (power spectra, correlation, histograms).

The properties of helium used in our analysis are taken from the work of McCarthy (1973). Figure 2 shows our experimental results for Nusselt number versus Rayleigh number up to $Ra = 10^{12}$. To span all this range we have used six different helium densities, whose corresponding pressures are 3, 8.5, 34, 138, 625 Torr and 2 atm. This allowed large overlap in the study. The calibration between upper and lower thermometers was checked for each pressure, with errors always smaller than 0.4 mK. We could thus be confident in results from temperature differences of $\Delta T \approx 3$ mK to $\Delta T \approx 1$ K, which represents more than two decades in Ra for each pressure.

As noted in Heslot *et al.* (1987) there are a variety of distinct differences between two turbulent regions: a region of 'soft' turbulence which lies in the range $2 \times 10^5 < Ra < 4 \times 10^7$ and a hard turbulence region which has been observed for $4 \times 10^7 < Ra < 6 \times 10^{12}$. One diagnostic for the difference is a histogram which plots the number of observations of a temperature T against T. For the centre probe, the histograms for the different regions show quite different signatures, with the soft region having a more Gaussian character, see figure 3(*a*) and the hard turbulence showing a more exponential character, see figure 3(*b*). The change in histograms (and other diagnostics) occurs rather abruptly around $Ra \sim 4 \times 10^7$. Hence this value will be the lower cut-off for most of our analysis. We use $Ra = 10^{12}$ as our upper cut-off since at higher Ra values the Prandtl number in our situation no longer remains substantially constant.

2.2. *Nusselt number dependence upon Rayleigh number*

In the selected range our measured Nusselt number can be very well fit in the form

$$Nu = N_0 Ra^{\beta}, \tag{2.1}$$

with

$$N_0 = 0.23 \pm 0.03, \tag{2.2}$$

$$\beta = 0.282 \pm 0.006. \tag{2.3}$$

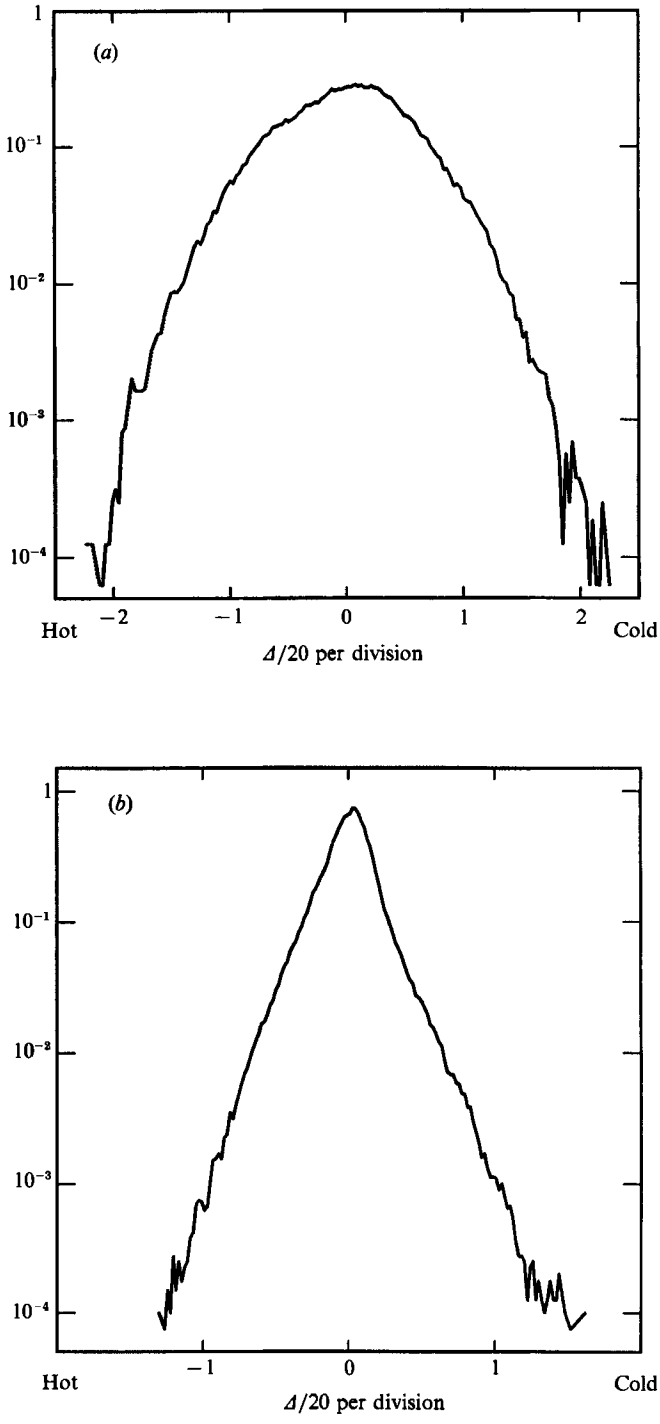

FIGURE 3. Histograms of the temperature distribution in the centre probe. (*a*) Soft turbulence regime, $Ra = 8.41 \times 10^6$. (*b*) Hard turbulence regime, $Ra = 1.47 \times 10^8$.

Note that the result differs from the classical $\beta = \frac{1}{3}$ in an apparently significant fashion (see table 1). To see this result in a broader context, we reviewed a number of experimental papers on convection in helium, air, and water. The aspect ratio (height over diameter) was variable and the Rayleigh numbers considered varied between 10^5 and 10^9. Most experiments yield an exponent β slightly below $\frac{1}{3}$ and are between 0.29 and 0.31 (Chu & Goldstein 1973; Garron & Goldstein 1973; Threlfall 1975; Fitzjarrald 1976). In some of these experiments the slope of the $\ln Nu$ *vs* $\ln Ra$ curve seems to inch upwards as Ra is increased. A relatively recent experiment showing that kind of behaviour was performed by Goldstein & Tokuda (1980). A similarity theory was offered by Long (1976) to predict the rate at which the law (1.9) would be approached. His theory is based on the matching of a small boundary layer with an interior of finite size. In this case a correction due to the scaling in the interior contributes to the thermal resistance of the box. This scaling of the interior flow depends on the temperature profile assumed to have the form

$$\langle T(z) \rangle \sim \Delta (z/z_1)^{-s}, \tag{2.4}$$

where Δ is a typical temperature scale in the interior, z_1 a typical height for a boundary layer and s an unknown index. Prandtl's theory is consistent with $s = \frac{1}{3}$. Malkus (1954, 1963) obtained $s = 1$ whereas Long (1975) expected $s = \frac{1}{2}$ from the analysis of some meteorological data. Using relation (2.4) Long obtains

$$(Ra/Nu^3)^{\frac{1}{4}} = C_1 - C_2 (Ra\,Nu)^{-s/4}, \tag{2.5}$$

where C_1 and C_2 are positive dimensionless constants. In figure 4(*a*) we show a fit to our data using the value $s = \frac{1}{2}$, suggested by Long, while in figure 4(*b*) we use $s = \frac{1}{3}$, the free fall value. A straight line fit would indicate satisfaction of (2.5). The data indicate a substantial deviation from a straight line and suggest that the power law form (2.1) with the non-classical exponent β is preferred.

We can also compare our Nusselt versus Rayleigh number results with previous experimental measurements, and with other theories. In doing this one must keep in mind the possibility that the Nu *vs.* Ra curve can depend upon the Prandtl number and also the shape of the container. In our case, Pr varies in the range 0.7 to 1.0 up to Rayleigh numbers of 2×10^{11} and then increases up to 1.5 at $Ra = 10^{12}$. The container is in the shape of a cylinder with aspect ratio (height/diameter) equal to one. Of all the previous experiments we have examined, Threlfall (1975) is the closest to ours in that he too used helium and a cylindrical geometry. He finds results in which for values of length/diameter equal to 0.4, 2.5 (in a preliminary experiment), 3 and 7 the Nusselt numbers are respectively 57.30, 108.7, 67.43 and 96.58 at Rayleigh number of 10^9. We find $Nu = 80$ at this Rayleigh number. It appears that Nu is non-monotonic with aspect ratio. (See also Deardorff & Willis (1965) who see a similar non-monotonic behaviour.) Given the likelihood of a non-monotone structure, we consider the agreement between our Nu and Threlfall's to be quite reasonable. One can directly compare our experimental results with the theory of Malkus (1954*b*, 1963). Since the boundary-layer thickness in that theory is determined by the local behaviour in its neighbourhood, the Rayleigh number for the boundary layer written in the form

$$Ra^{\mathrm{bl}} = \frac{Ra}{16Nu} \tag{2.6}$$

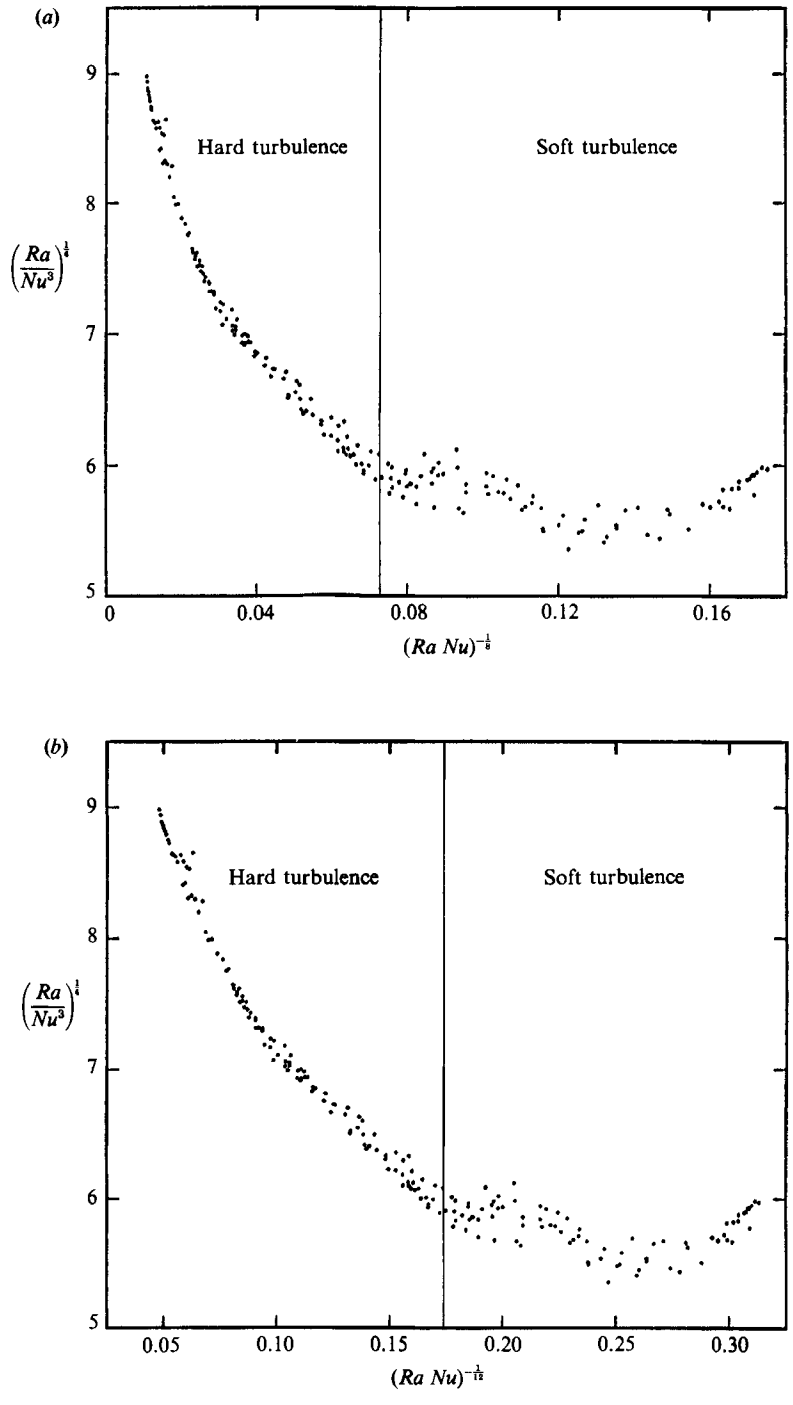

FIGURE 4. The dependence of the heat flux on the temperature difference is plotted using the variables $(Ra\,Nu)^{-s/4}$ and $(Ra/Nu^3)^{\frac{1}{4}}$. In (*a*) $s = \frac{1}{2}$, in (*b*) $s = \frac{1}{3}$. A straight-line fit would indicate agreement with Long's result (see text).

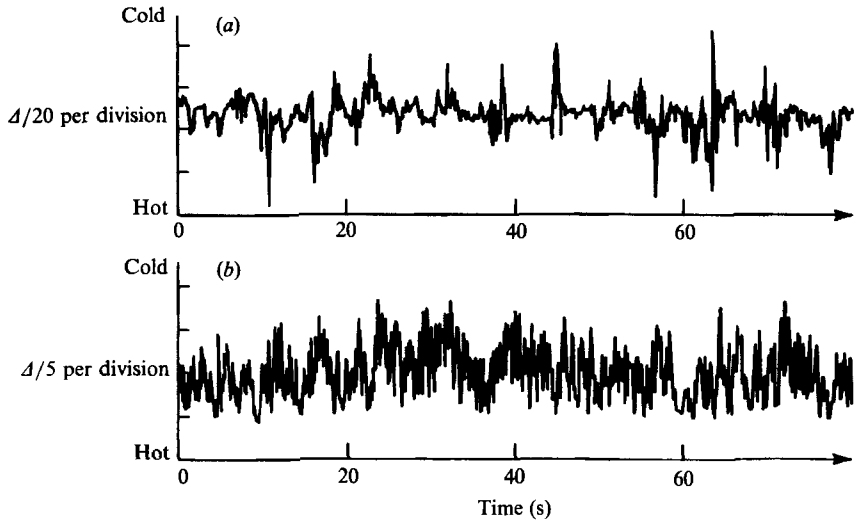

FIGURE 5. Time recording of the temperatures at the centre (*a*) and bottom (*b*) probes in the hard turbulence regime, $Ra = 1.2 \times 10^9$.

has a particularly simple behaviour. In fact, for any box with a constant cross-section, $Ra_{\rm bl}$ should be only a function of Prandtl number, and be quite independent of box shape and other details. In symbols

$$Ra^{\rm bl} = F(Pr). \tag{2.7}$$

On the other hand, our theory (developed below) suggests that the boundary-layer thickness is determined by a fluctuating wind near the boundary layer so that

$$Ra^{\rm bl} = G(Pr, \ldots) Ra^{\frac{1}{7}}, \tag{2.8}$$

where G depends upon such 'details' as the box shape and aspect ratio. The work of Goldstein & Chu (1969) does not support equation (2.7), but because the aspect ratio is changing it cannot test (2.8). The work of Townsend (1959) is in fact consistent with (2.7) (see Malkus 1963) but the range of estimated $Ra (3 \times 10^8 < Ra < 7 \times 10^8)$ is too small to be definitive. (Moreover, Townsend's 'box' does not have a top. This open geometry will probably have a very different flow pattern from that in a closed box.) On the other hand, our data gives $Ra^{\rm bl}$ equal to 76, 127, 256, and 361 for Rayleigh numbers respectively 4×10^7, 10^9, 10^{11} and 10^{12}. These data, if taken at their face value, rule out (2.7) and suggest the incompleteness of the theory upon which it is based. At least they do push one towards looking for another theoretical approach.

2.3. *Experimental evidence for scaling behaviour*

Figures 5 and 6 show time recordings for the centre and bottom bolometers at two different Rayleigh numbers 1.2×10^9 and 2×10^{11}. The centre bolometer signal is characterized by a distribution of sharp peaks of variable heights. A simple observation of the two recordings shows that the fluctuation amplitude decreases as Ra increases (the vertical scale is expressed relative to the total temperature difference Δ). In a later paper we intend to focus on the detailed correlation of the time signals. Here we focus upon a few properties needed to characterize the overall properties of the turbulent flow in different regions of the cell. In particular we look

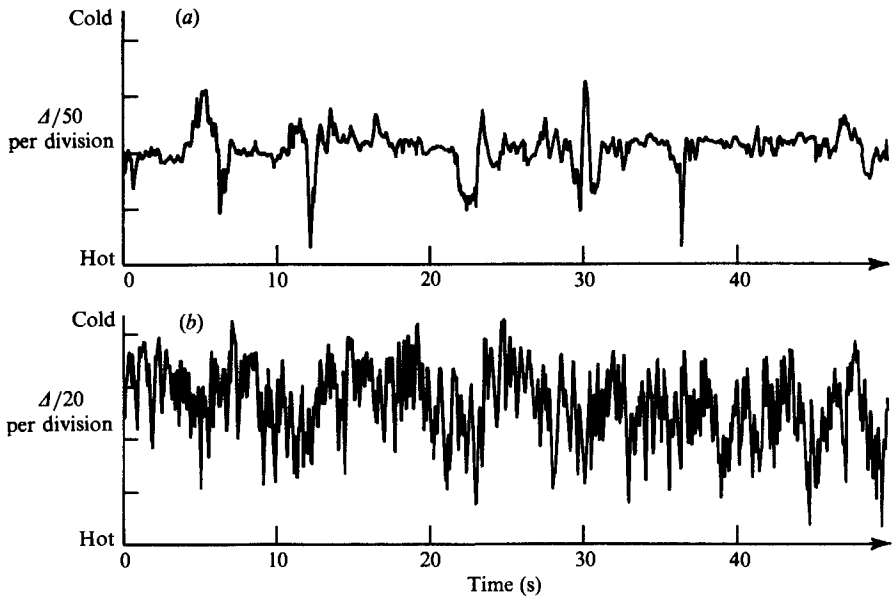

FIGURE 6. Time recording of the temperatures at the centre (*a*) and bottom (*b*) probes in the hard turbulence regime, $Ra = 2 \times 10^{11}$.

for histograms which depict the number of times a given temperature T is observed for each of the bolometers. Figure 7 shows two such histograms for different Rayleigh numbers each taken from the bottom bolometer. This bolometer is in a fixed position 200 μm above the bottom plate. We interpret the marked change in terms of the boundary layer which we believe to exist near the cell walls. If this boundary layer is conductive or viscous in character its thickness λ should be given by the estimate (Kraichnan 1962)

$$\lambda \sim L/Nu. \tag{2.9}$$

(We use two different notations for the size of the thermal boundary layer in this paper: λ is used almost always, but the notation z_1 is used to connote our use of the classical similarity theory instead of our new model.) From this estimate, for the lower of the two Rayleigh numbers the probe will be just within the boundary layer while for the higher Rayleigh number it will fall outside the boundary layer. In these histograms one can clearly see large low-temperature excursions inside the boundary layer (figure 7*a*), and large high-temperature excursions when the probe is outside the bottom boundary layer (figure 7*b*).

We have measured the average temperature in this bottom probe as a function of Nusselt number. These data are shown in figure 8. One might wish to use (2.9) to interpret these data in terms of a measurement of temperature as a function of scaled height

$$z/\lambda = Nu\, z/L, \tag{2.10}$$

where $z = 200$ μm is the height of the probe and $L = 8.7$ cm is the height of the cell. Note however that the results in figure 8 are averages over a probe which has a characteristic diameter of order 100 μm. At the smallest Rayleigh number, this size is negligible in comparison to the boundary-layer width. Hence for the larger Rayleigh numbers in figure 8, one must consider that this figure gives a spatial average and not a local measurement. For this reason, we are not in a good position

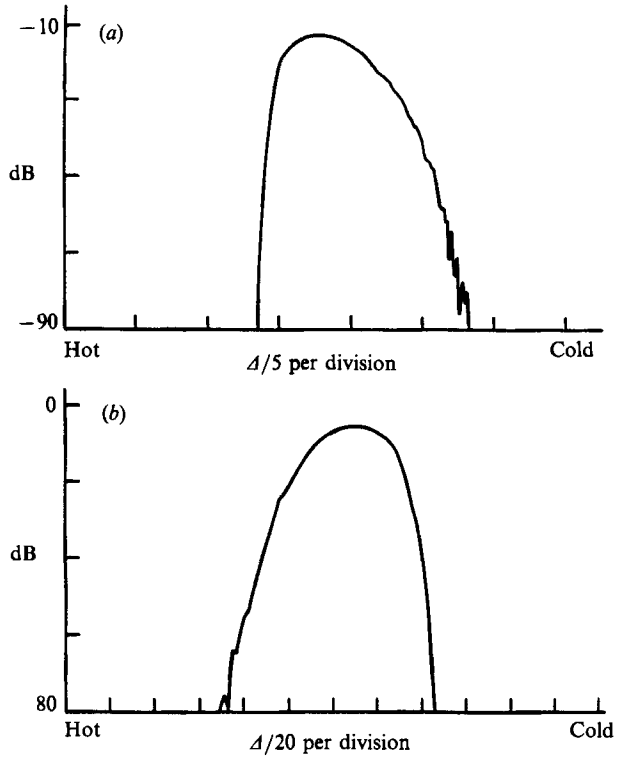

FIGURE 7. Histograms of the temperature distribution measured at the bottom bolometer. On (*a*), the bolometer is in the thermal boundary layer, $Ra = 1.2 \times 10^9$, and there are rare, colder excursions. On (*b*), the bolometer is out of the boundary layer, $Ra = 2 \times 10^{11}$, and there are relatively rare, hot excursions.

to compare our results for average temperature with previous theoretical (e.g. Malkus 1963) or experimental (e.g. Townsend 1959) results. Notice that Malkus' theory does fit the detailed shape of Townsend's average temperature profile near the wall. Our scaling theory, described below, cannot match this achievement, but it does provide a better fit to other portions of our data (e.g. the Rayleigh–Nusselt curves).

The signals in the bottom probe have a larger frequency range than those in the centre probe. These also show a somewhat intermittent signal at a frequency which we call ω_p. This oscillation is clearly seen in the recording shown in figure 9 at $Ra = 2.3 \times 10^8$ taken in a time period where it is present with a large amplitude. It represents the envelope with about 8 periods present. The Fourier spectrum is shown in figure 10. This oscillation frequency ω_p scales with Rayleigh number like

$$\frac{\omega_p L^2}{\kappa} = N_1 Ra^{\delta}, \tag{2.11}$$

$$N_1 = 0.36 \pm 0.01, \tag{2.12}$$

$$\delta = 0.491 \pm 0.002. \tag{2.13}$$

These data have been placed in table 1. Figure 11 shows a plot of the data used to generate the fit (2.11).

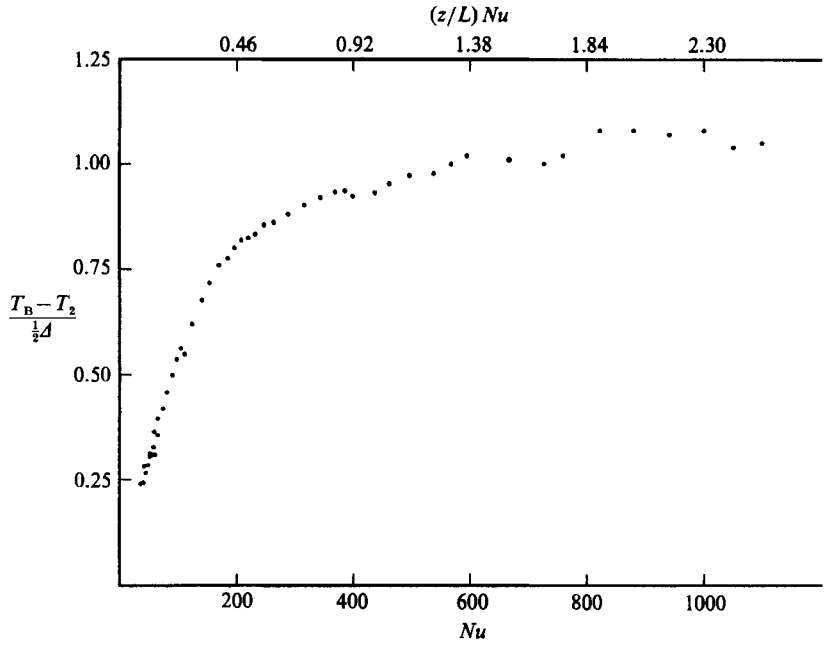

FIGURE 8. The average temperature in the bottom probe *vs.* the Nusselt number. This provides an indirect measurement of the drop in average temperature as one departs from the bottom. Here T_2 is the temperature in the bottom plate. The top scale provides an estimate of z (probe position) divided by λ (boundary-layer thickness).

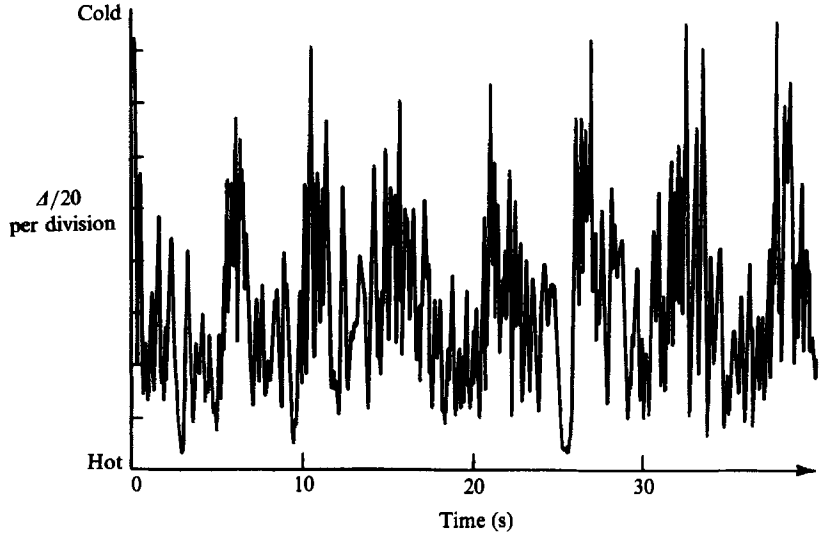

FIGURE 9. A time series from the bottom probe, showing 8 oscillations at the characteristic frequency ω_p. Here $Ra = 2.3 \times 10^8$.

The scaling of (2.11) might be compared to the characteristic frequency predicted by Howard (1966). In the boundary layer his point of view gives a frequency proportional to κ/λ^2 so that, applying his approach, we could conclude that the right-hand side of (2.11) should behave as a Rayleigh number to a two-third power. The experiment appears to rule out this possibility.

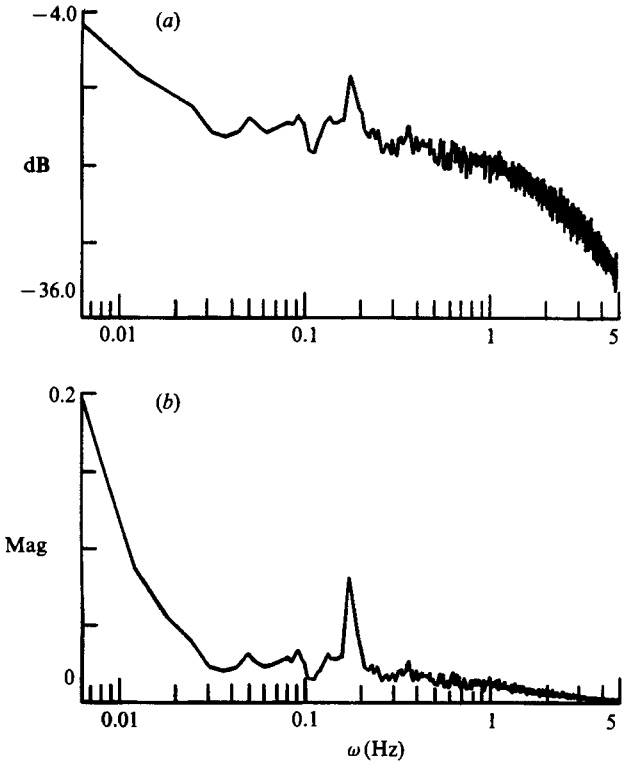

FIGURE 10. Power spectrum from the bottom probe at $Ra = 2.3 \times 10^8$, showing the peak at the characteristic frequency ω_p. The ordinate on plot (*a*) is given in a logarithmic scale, in plot (*b*) it is in a linear scale.

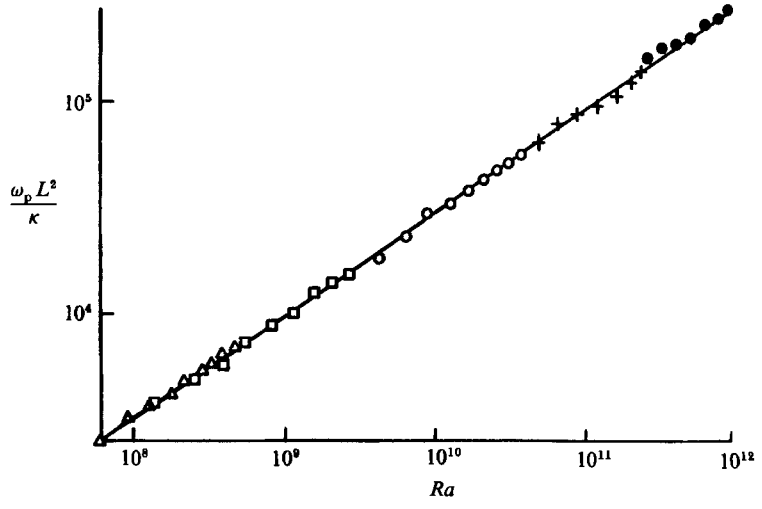

FIGURE 11. The dependence of the characteristic frequency ω_p upon Ra. The different symbols indicate different helium pressures within the cell.

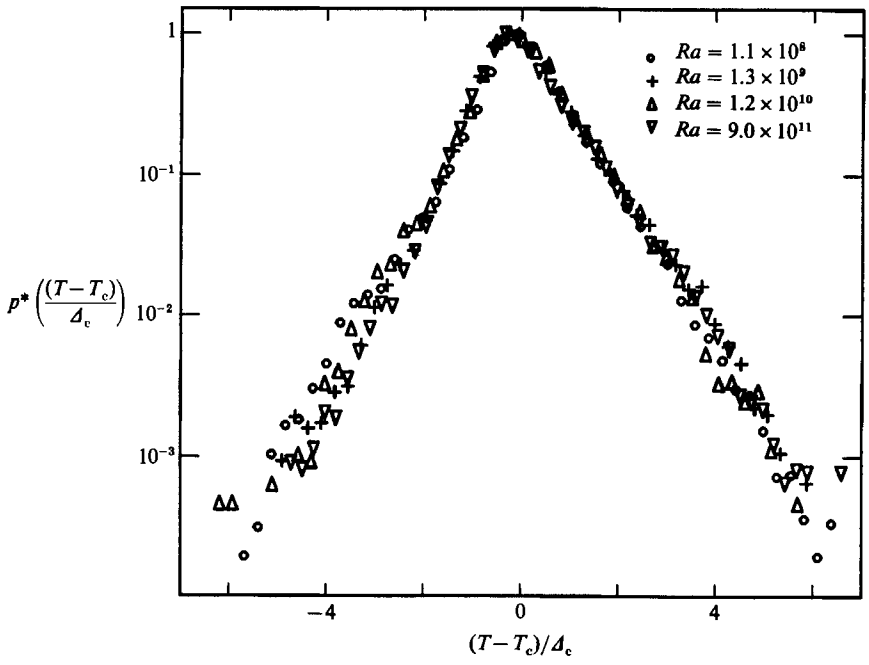

FIGURE 12. Comparison of histograms of the temperature fluctuation in the centre. The number of times a given temperature is observed is plotted against this temperature. For various Rayleigh numbers the histograms are all rescaled so that the r.m.s. temperature fluctuations coincide.

The most striking evidence for universality in the hard turbulence regime is shown by the histograms of the temperature of the central probe. In figure 12 we show histograms which give the probability $p(T)\,\mathrm{d}T$ that one will observe a temperature between T and $T+\mathrm{d}T$ in the central probe. Data for four values of Ra are given. The pictures are superposed by setting independently in each a zero of temperature, T_0, and a temperature scale, Δ_c, so that

$$p(T) = \Delta_c^{-1} p^*\left(\frac{T-T_0}{\Delta_c}\right), \tag{2.14}$$

where p^* is a universal function which is independent of Ra but might depend on Pr. T_0 and Δ_c are temperature scales that depend on Ra and Pr. The wings of the universal function p^* are well approximated, in the semi-logarithmic plot of figure 12, by straight lines albeit with different slopes on the hot side and on the cold side. This universality is a very striking result. Equally striking is the simple power-law behaviour of the typical temperature in the central region. In figure 13 we plot the standard deviation of the temperature fluctuation, $T-T_0$, as a function of the Nusselt number. The latter is proportional to the Δ_c of (2.14). We next fit this curve as

$$\Delta_c/\Delta = N_3 Nu^{\sigma}, \tag{2.15}$$

$$\sigma = -0.52 \pm 0.01, \tag{2.16}$$

$$N_3 = 0.17 \pm 0.02. \tag{2.17}$$

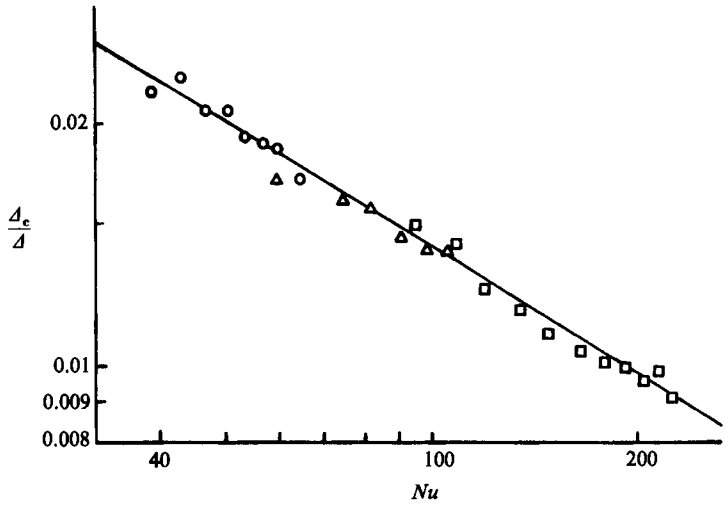

FIGURE 13. The dependence of the characteristic temprature Δ_c on Nu. Δ_c is proportional to a r.m.s. temperature fluctuation and is measured at the centre probe. The different symbols indicate different pressures in the helium.

Classical theory gives $\sigma = -s$ while the experimental result points to $\sigma = -\frac{1}{2}$. The result of substituting (2.1) into (2.15) is shown in table 1 and gives

$$\Delta_c/\Delta = N_4 Ra^{\gamma}, \tag{2.18}$$

$$\gamma = -0.147 \pm 0.005, \tag{2.19}$$

$$N_4 = 0.36 \pm 0.04. \tag{2.20}$$

3. Scaling theory

3.1. *A review of theoretical analyses*

We believe that the experimental situation can be well described by the Boussinesq approximation, in which the flow equations read

$$\left.\begin{aligned} \boldsymbol{u}_t + \boldsymbol{u}\cdot\nabla\boldsymbol{u} &= \nu\nabla^2\boldsymbol{u} - \nabla p + g\alpha T\hat{\boldsymbol{z}}, \\ T_t + \boldsymbol{u}\cdot\nabla T &= \kappa\nabla^2 T, \\ \nabla\cdot\boldsymbol{u} &= 0, \end{aligned}\right\} \tag{3.1}$$

together with boundary conditions which set the velocity equal to zero on the walls. We envisage a set of thermal boundary conditions which set the temperature equal to $\pm\frac{1}{2}\Delta$ at the bottom/top plates and the normal derivative of temperature equal to zero at the sidewalls.

In what follows, we shall write the coordinate and velocity vectors as (x, y, z) and (u, v, w) with z and w being upward components.

There is one possible problem about the use of these Boussinesq equations. They are quite symmetrical under the exchange of top and bottom, and a flip in the sign of w and T. The histogram of figure 12 is not exactly symmetrical under $T \leftrightarrow -T$. We think that this lack of symmetry is a consequence of the natural symmetry breaking which will put a single convective roll in a cell of aspect ratio unity, together with a pinning of that roll by the leads holding the bolometers.

The next step is to state a similarity analysis which defines the order of magnitude of the different quantities which appear in (3.1) in different regions of the cell. We start from the presupposition that the hard turbulence regime can be well described by simple power laws, as in table 1, equations (2.1), (2.11) and (2.15), and by a universal behaviour as shown in figure 12. The non-classical value of β found in our experiment (and previous ones) suggests an important departure from the classical point of view concerning the boundary layer in this system. The classical result, $\beta = \frac{1}{3}$, emerges if one considers in a direct fashion the stabilization of an isolated boundary layer. Our result, $\beta < \frac{1}{3}$, gives a boundary layer which is, in the limit of high Rayleigh number, too thick to exist in isolation.

We take this result seriously and propose that the boundary layer is not self-stabilized but rather gains stability from randomly directed winds which blow across it. The stability of the boundary layer is investigated in a detailed calculation in §4.

This produces a very important difference from the classical theory. In the latter the stability of the boundary layer determines the heat flux at the leading order. In our view stability is irrelevant because the boundary layer can always be stabilized by the wind. This leaves open the problem of theoretically determining the heat flux: another kind of balance has to be found to determine β.

In the central or interior region of the cell, we envisage motions on many scales up to that of the entire cell, consisting of convective eddies, and of thermals and plumes (Turner 1969). These motions have been visualized by many previous experiments (e.g. Krishnamurti & Howard 1981; Chu & Goldstein 1973). In our view, the interior motion has two major effects; it carries heat towards the top of the cell and produces winds with an appropriate velocity to stabilize the boundary layer.

The theoretical analysis must then connect the interior behaviour with that of the boundary layer. This connection is two-fold. First, we require that the convection of temperature fluctuations of order Δ_c in the central region produces a heat flux equal to the heat flux across the boundary layer. An additional matching condition requires that the hot (or cold) pieces which break off the bottom (or top) boundary layer are accelerated to an appropriate speed so that they can smoothly merge into the all-over flow in the central region. To achieve this merging we make the rather bold (and heuristic) assumption that there exists a mixing zone in which fluid is accelerated to the velocities of the central region. This zone (see figure 14) is assumed to be much thicker than the boundary layer, but thin compared to the height of the cell. In our mathematical analysis of the mixing zone, we assume that the characteristic lengthscales, timescales, velocities, and temperature distributions in the mixing zone are those appropriate to achieve an interpolation between the interior and the boundary layer. We then balance buoyancy force against viscous drag and obtain one more relation between the quantities describing the central region and those of the boundary layer. This analysis is carried out in §3.2 below. In this way, we derive the values of the quantities, β, γ and ϵ shown in the 'present paper' theory column in table 1.

Section 3.3 then gives a more detailed description of the presumed behaviour of the mixing zone. In §3.4, the dynamics of the mixing zone is used to explain the exponential character of the histogram in figure 12. Finally, the stratifications in the mixing zone are used to describe the nature of the observed oscillations and their characteristic frequency, ω_p.

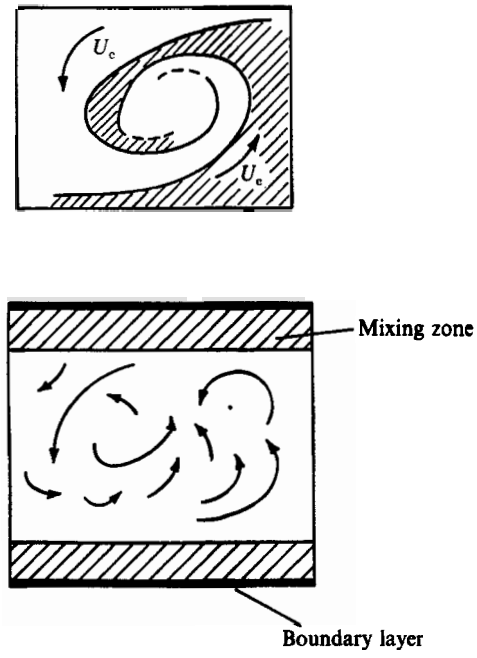

FIGURE 14. Two possible cartoons of the flow pattern in the centre of the cell.

3.2. *Different regions, different behaviours*

In our analysis we distinguish three regions of different widths (see figure 14): a central region that occupies most of the box, a mixing zone of small width d_m and an even smaller boundary layer of thickness $\lambda \ll d_m$. In the latter, heat is transported by conduction alone. The central region is also where the experimental data are most universal. We hence begin the presentation of the theory in this region where its conclusions can most easily be verified experimentally. We then deal with the boundary layer and match it to the central region. The matching is made through a mixing zone which we will describe in more detail in the next section.

We now offer a heuristic depiction of the geometry of the flow. Figure 14 shows two possible cartoon views of the geometry of the different regions. They are different but either cartoon is consistent with the scaling analysis given below. That analysis is based upon balancing the order of magnitude of various terms in the hydrodynamic equations and would be consistent with a variety of geometric interpretations. We simply do not know the correct geometry of the flow.

The theory in the central region is the classical similarity theory. We assume there is a flow of typical velocity scale u_c, lengthscale L and temperature scale Δ_c. Thermal and momentum diffusivities are small as compared to turbulent mixing and drag, and hence neglected. The only dimensionally correct relation is then

$$u_c \sim (\alpha g L \Delta_c)^{\frac{1}{2}}. \tag{3.2}$$

Another assumption is needed, namely that the whole central region is filled with regions of typical velocity u_c and temperature Δ_c. This implies

$$H \sim u_c \Delta_c. \tag{3.3}$$

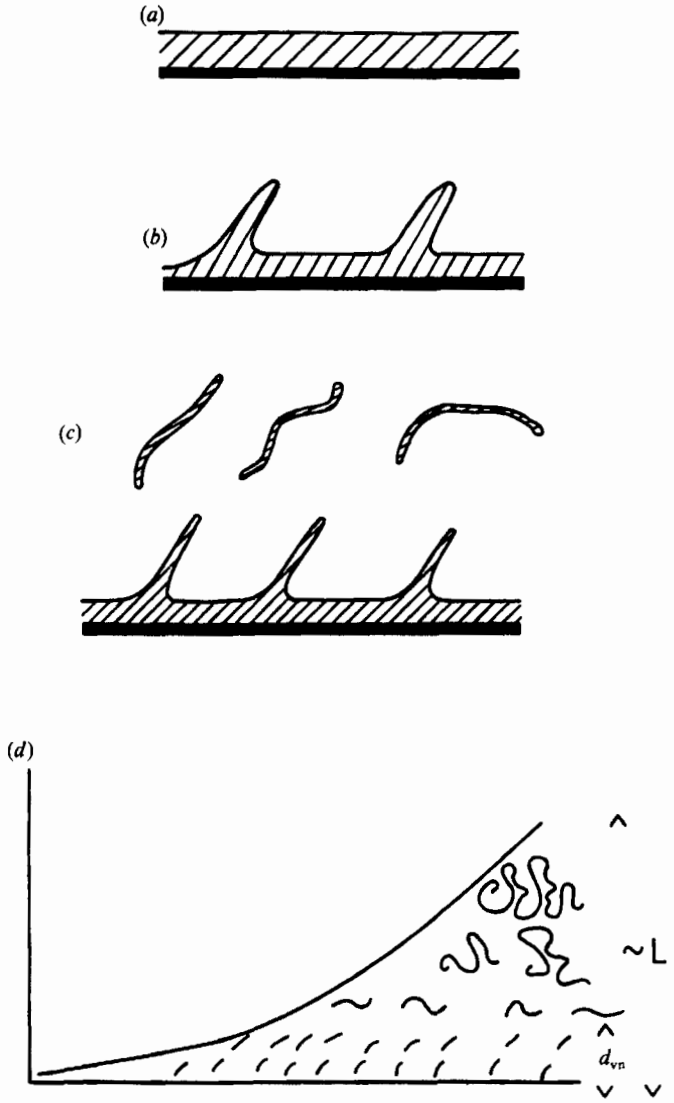

FIGURE 15. The mixing of the hot fluid from the boundary layer with the flow in the interior. (*a*) A boundary layer of size λ, stabilized by the wind, is formed (the dark line represents the bottom plate). (*b*) When the wind changes, the layer is unstable and breaks in a way similar to the Rayleigh–Taylor instability. (*c*) The process repeats itself. The spikes can be deformed by the wind, but the fraction of hot bubbles or objects is essentially determined by their speed of rise (see text). (*d*) The entire region, cold and hot fluid together is aspired into the interior by turbulence in the interior. The hot region may be deformed further in the process but the fraction of hot and cold fluid remains the same.

We continue to leave out factors of order unity. Recall that in §2 we defined a number of scaling indexes through the relations $Nu \sim Ra^{\beta}$, $\Delta_c \sim Ra^{\gamma}\Delta$ and $u_c \sim Ra^{\epsilon}\nu/L$. From (3.2) and (3.3) we get the relations between exponents:

$$\epsilon = \tfrac{1}{2}(1+\gamma), \quad \gamma = \tfrac{2}{3}(\beta - \tfrac{1}{2}). \tag{3.4}$$

These relations are well verified in the experiment as shown in table 1. To introduce a different scaling, one would need to assume that the thermals fill only a vanishing

fraction of the space, at large Ra. This is ruled out by the temperature distributions obtained in the experiment: a large region near zero temperature would appear as a spike in the distribution shown in figure 12.

We assume that most of the temperature drop occurs over the width of the boundary layer. This is a reasonable assumption: buoyancy driven motions tend to improve transport over purely conductive transport. Hence they require smaller gradients for the same amount of heat flux. We call λ the width of the conductive layer. The heat flux is then given by (1.7) and hence

$$\lambda \sim \frac{\kappa \Delta}{H} \sim Ra^{-\beta} L. \tag{3.5}$$

At this stage, we have but one unknown, β. To find β we assert the existence of a mixing zone which interpolates between the extreme temperature differences in the boundary layer and the much milder fluctuations in the central region. We assume that this zone contains two kinds of fluids. In particular the bottom mixing zone contains a large fraction of tepid fluid which has a temperature distribution similar to that of the central region and a much smaller fraction f of small regions of very hot fluid which have entered from the bottom boundary layer (see figure 15). We assume further that the hot fluid retains many of the characteristics of the bottom boundary layer as shown in figure 15. In our cartoon view, the fluid is arranged in sheets which retain a thickness similar to the boundary-layer thickness λ. They move upward under the influence of buoyancy forces until their speed is high enough so that viscous forces can balance buoyancy. At that point they have a velocity

$$w_h = g\alpha \Delta \lambda^2 / \nu. \tag{3.6}$$

One further assumption is needed. We assert that the velocity w_h is just the right speed so that the hot sheets can merge into the central region flow, with its characteristic velocity u_c. Then we write (3.6) as

$$u_c \sim g\alpha \Delta \lambda^2 / \nu. \tag{3.7}$$

Now we have enough equations to estimate everything. Solve equations (3.7), (3.5) and (3.4), assuming that the Prandtl number is of order unity. One then finds $\beta = \frac{2}{7}$, and from (3.4) one gets $\gamma = -\frac{1}{7}$, and $\epsilon = \frac{3}{7}$. Those are the theoretical values used in table 1.

3.3. *More detailed description of mixing zone*

We take the upward component of the velocity of the hot fluid to be the same as in the previous estimate (3.6). However these sheets or objects are in a highly unstable configuration. After a time, turbulent mixing will rip the sheets to pieces as in the figure 15. We wish to estimate the fraction f of the volume eventually occupied by hot fluid. To do this, notice, that if the fluid enters from the boundary layer at an upward speed w_b and is accelerated upwards to the speed w_h, then by conservation of the flux the fraction of the fluid which is hot at the height of high speed, is given by

$$w_h f \sim w_b. \tag{3.8}$$

We can estimate w_b by saying that, at the top of the boundary layer conductive and convective heat flow are of the same order so that the heat flux is

$$H \sim \kappa \Delta / \lambda \sim w_b \Delta. \tag{3.9}$$

In this way we estimate the hot fraction as

$$f \sim \frac{\kappa\nu}{\lambda^3 g\alpha\Delta}. \tag{3.10}$$

In the next stage the hot layers become unstable and shatter (see figure 15). As this occurs they mix with the surrounding fluid and spread into finely divided hot droplets or sheets. We assume that this finely divided material is aspired by the fast moving central flow and advected into the central region. The finely structured fluid in the mixing zone may be considered equivalent to a homogeneous fluid of temperature

$$\Delta_m = f\Delta. \tag{3.11}$$

To close the description of hard turbulence requires the matching of the temperature of the mixing region with the temperature of the central region. At this point the present theory is in contradiction with free fall theory. Free fall theory pictures the formation of plumes or thermals out of the mixed fluid at temperature Δ_m. These plumes then accelerate upward while they lose some temperature. In the present theory we assume instead that the thermals are engulfed in a large-scale flow of velocity u_c in the interior. While the mixture is advected by this flow its temperature does not change significantly any more and instead of the temperature drop described by (1.4) we get

$$\Delta_c = \Delta_m, \tag{3.12}$$

so that we can now evaluate Δ_c as

$$\Delta_c \sim \frac{\kappa\nu}{\lambda^3 g\alpha}. \tag{3.13}$$

Equations (3.2), (3.3), (3.5) together with (3.13) yield once more the values of β, γ and ϵ used in table 1. Notice that the derivation given here is slightly different from the one given in the previous section, but yields identical results. We consider this second derivation physically more sound. Indeed it is more satisfactory to assume an equality of temperatures (3.12) than an equality of speeds ((3.2), (3.6)) because it is possible to expect that such an equality of temperatures will be produced by a very efficient turbulent mixing.

To find the width of the mixing zone, d_m, we notice that once a sheet detaches itself from the boundary layer it accelerates to the velocity w_h as above while the boundary layer refills with cold fluid. Then it accumulates heat during a time

$$\tau_s \sim \lambda^2/\kappa, \tag{3.14}$$

after which it is ready to emit a new sheet. The actual time after which the new sheet is emitted may fluctuate widely around this average value. After this time the first sheet has travelled a distance d_m given by

$$d_m \sim w_h \tau_s, \tag{3.15}$$

which yields

$$d_m \sim \frac{g\alpha\Delta\lambda^4}{\kappa\nu}. \tag{3.16}$$

Two successive sheets are separated by cold fluid coming from the central region (see figure 15). The fraction of hot fluid in the whole structure drifting upward is

$$f \sim \lambda/d_m, \tag{3.17}$$

in agreement with (3.10). Note that in this argument the height d_m is actually the initial separation between sheets. The actual height over which the fluid will be well mixed is not relevant at this point of the discussion. Even if it were of order L the argument would stand unchanged. We can offer only conjectures here. For example, mixing layers that might encircle the entire box give a situation like the one of figure 14 where zones of coherent temperature $+\Delta_m$ and $-\Delta_m$ wrap around the box. By substituting (3.12) with (3.11), and (3.17) we find the result

$$d_m \sim \lambda \frac{\Delta}{\Delta_c}, \tag{3.18}$$

so that, as expected, $d_m \gg \lambda$. In fact, from the estimate $\lambda \sim L/Nu$, and the data in table 1, (3.18) implies that d_m is of order L at the soft–hard transition.

3.4. *The mixing zone: exponential distributions and oscillations*

The fact that temperature distributions are exponential is a striking characteristic of the hard turbulence regime. Yet models that predict log-normal distributions or distributions with algebraic tails are more common in turbulence theory than models producing exponential laws. Classical theories, for instance, in which the thermals expand and cool by mixing with new fluid as they rise often model the cooling as a multiplicative process. This would yield algebraic tails to the probability distributions, which are not observed. To explain the exponential distribution we assume that the warm mixing zone forming near the bottom of the box is aspired intermittently by the central flow. Between these aspiration events the mixing zone is heated at a constant rate H and its temperature grows as

$$T_m(t) \sim H_m \times (t - t_a)/d_m, \tag{3.19}$$

where t_a is the time at which the latest aspiration took place, H_m is the average heating rate of the cooler fluid in the mixing zone and d_m is the thickness of the mixing zone. Now consider the timing of aspiration events. There is some regularity in the distribution of those events. For sufficiently long waiting times however the memory of the previous event is lost. As a result the tail of the waiting time distribution is exponential as in a Poisson distribution of points on the same axis. It is actually quite reasonable for a chaotic central region that the aspiration of a piece of the mixing zone is a randomly distributed event. From the exponential distribution of waiting times an exponential distribution of temperatures T_m follows.

The difference between the two slopes for positive and negative values of $T - T_0$ in figure 12 can be tentatively explained as a result of the directed eddy motion shown in figure 14(*a*). The fluid moved into the central region via aspiration events in the upper mixing zone has to travel much further to reach the probe than the fluid coming from below. We expect that the former is cold and the latter hot. Hence the temperature of the hot fluid will be moderated to a much smaller degree than that of the cold fluid. Thence the distribution is skewed towards the hotter side.

Exponential distributions have been observed in several other turbulent fluid flows. It would be interesting to know whether the present model can also be applied to other experiments. In the present experiment an exponential distribution of waiting times between major temperature fluctuations has also been observed and it would be interesting to know if events with similar waiting time distributions can be observed in other situations and related to an exponentially distributed variable.

We now turn to the analysis of the oscillation frequency ω_p. For this analysis we require the width of the mixing zone, d_m. The turbulent advection of the central fluid

at temperature Δ_c can create regions of inverted gradient, with the hot fluid on top of the cold fluid (see our cartoon view in figure 14). Experimental measurements associate the frequency ω_p with the mixing layers. This suggests the use of d_m as a characteristic length of the regions of inversion. The inverted gradient is then Δ_m/d_m and waves of length d_m will oscillate in this adverse gradient with the Brunt–Väisälä frequency (Väisälä 1925; Brunt 1927)

$$\omega_{BV} = \left(\frac{g\alpha\Delta_m}{d_m}\right)^{\frac{1}{2}}.$$

From (3.12), (3.18) and (3.5) one gets

$$\omega_{BV} \sim Ra^{\frac{1}{2}}. \tag{3.20}$$

This frequency scales with Ra just as the frequency ω_p observed in the experiment, and we thus get $\delta = \frac{1}{2}$. It is of an entirely different nature than the frequency predicted by Howard (1966) and observed in some experiments at higher Prandtl numbers.

4. The stability of the boundary layer

In this section we present a linear stability analysis of the boundary layer. The stability of the boundary layer is an important problem because our theory suggests that the size of the boundary layer grows so rapidly that it would become unstable with respect to thermal convection. Indeed as shown in (2.8) the Rayleigh number of this layer grows asymptotically. This is in contradiction with the hypothesis of marginal stability of the boundary layer (Howard 1966). In our analysis we also assume that the boundary layer is marginally stable, but the stability analysis must involve a shearing wind. The effect of a shearing wind on convection was investigated in an experiment of Ingersoll (1966). He observed a decrease of the Nusselt number when a moderate shear was imposed and attributed it to the stretching and breaking of the temperature carrying eddies by the shear. Theoretical work by various authors also confirms the existence of this effect for a horizontal Poiseuille flow in a layer heated from below (Datta 1965; Hughes & Reid 1967; Gage & Reid 1968). The influence of shear on the stability of reacting systems was also studied by Spiegel & Zaleski (1984). It was found that shear was stabilizing at large wavenumber but could be destabilizing at small wavenumbers. In this work we numerically investigate the effect of a plane Couette flow. We describe this analysis in a rather detailed way and derive a stability condition for the boundary layer. We then return to our scaling theory and show that this condition is always realized. The system of linearized Boussinesq equations about a wind of horizontal speed $\boldsymbol{u}_0(z) = \tilde{u}_0(z)\,\hat{\boldsymbol{x}}$ is

$$\left.\begin{aligned} \boldsymbol{u}_t + \boldsymbol{u}_0\cdot\nabla\boldsymbol{u} + w\boldsymbol{u}_{0,z} &= \nu\nabla^2\boldsymbol{u} - \nabla p + g\alpha T\hat{\boldsymbol{z}}, \\ T_t + \boldsymbol{u}_0\cdot\nabla T - (\Delta/\lambda)\,w &= \kappa\nabla^2 T, \\ \nabla\cdot\boldsymbol{u} &= 0, \end{aligned}\right\} \tag{4.1}$$

Boundary conditions are

$$T(x,y,0) = \Delta, \quad T(x,y,\lambda) = 0. \tag{4.2}$$

For the velocity, there can be no-slip

$$u = v = w = 0 \quad \text{for } z = 0, \lambda, \tag{4.3}$$

or slip

$$w = 0, \quad w_{zz} = 0 \quad \text{for } z = 0, \lambda. \tag{4.4}$$

To write (4.1), (4.2) and (4.3) in non-dimensional form we use λ as the unit of length, λ^2/κ as the unit of time, and Δ as the unit of temperature. $Ra^{\mathrm{bl}} = g\alpha\Delta\lambda^3/\nu\kappa$ is then the boundary-layer Rayleigh number while $Re = \lambda\tilde{u}_0/\nu$ is the shear-flow Reynolds number

$$u_t + Pr\,Re\,\tilde{u}_0\,u_x + Pr\,Re\,\tilde{u}_{0,z}\,w = Pr\,\nabla^2 u - p_x, \tag{4.5}$$

$$w_t + Pr\,Re\,\tilde{u}_0\,w_x = Pr\,\nabla^2 w - p_z + Pr\,Ra^{\mathrm{bl}}T, \tag{4.6}$$

$$T_t + Pr\,Re\,\tilde{u}_0\,T_x - w = \nabla^2 T, \tag{4.7}$$

$$u_x + w_z = 0. \tag{4.8}$$

The variables u, w and p can be eliminated from the stability equations, leaving an equation for T alone. We look for solutions of the form

$$T(x,z) = \mathrm{Re}\,[\theta(z)\exp(\mathrm{i}k(x-c't))], \tag{4.9}$$

where $\theta(z)$ is an unknown complex function. Re, Im mean, respectively, the real and imaginary part. It is convenient to take $c' = Pr\,Re\,c$ where c is an unknown complex eigenvalue or complex wave speed $c = c_{\mathrm{r}} + \mathrm{i}c_{\mathrm{i}}$. Instability occurs when an eigenvalue with imaginary part $c_{\mathrm{i}} > 0$ is found. A sixth-order equation for θ is obtained through elimination of u, v and p,

$$L_4 L_2 \theta + Ra\,Pr\,k^2\theta = 0, \tag{4.10}$$

where

$$L_4 = -\mathrm{i}k\,Pr\,Re\,[(\tilde{u}_0 - c)(\mathrm{D}^2 - k^2) - u_{0,zz}] + Pr\,(\mathrm{D}^2 - k^2)^2,$$

$$L_2 = -\mathrm{i}k\,Pr\,Re\,(\tilde{u}_0 - c) + (\mathrm{D}^2 - k^2),$$

and where we use the notation $\mathrm{D} = \mathrm{d}/\mathrm{d}z$. The boundary conditions can be rewritten in terms of θ. There are six of them, of the form $A_i(\theta) = 0$ for $i = 1$ to 6:

$$\left.\begin{aligned} A_1(\theta) &= \mathrm{Re}\,\theta, \quad A_2(\theta) = \mathrm{Re}\,[L_2\theta], \quad A_3(\theta) = \mathrm{Re}\,[\mathrm{D}L_2\theta], \\ A_4(\theta) &= \mathrm{Im}\,\theta, \quad A_5(\theta) = \mathrm{Im}\,[L_2\theta], \quad A_6(\theta) = \mathrm{Im}\,[\mathrm{D}L_2\theta]. \end{aligned}\right\} \tag{4.11}$$

For $Pr = 1$ the problem is identical to the stability analysis of a circular Couette flow between cylinders rotating at approximately the same speed with an axial flow $\tilde{u}_0$. This problem has been treated for the case of a Poiseuille flow $\tilde{u}_0$ by Datta (1965), and Hughes & Reid (1967). Datta made a small Re expansion whereas Hughes & Reid started from large Re. Gage & Reid (1968) summarized these results and discussed their application to three-dimensional stability and shear flow. It results from the analysis of Reid and his coworkers that for $Re < 5400$ the shear stabilizes convection rolls normal to the direction of shear in surprising agreement with the small-Re result of Datta,

$$Ra_{\mathrm{c}} = 1708.8 + 1.32\,Re^2. \tag{4.12}$$

Why this small-Re result is valid over several orders of magnitude is not well understood. At $Re = 5400$ the viscous instability of Poiseuille flow sets in. We have not found many other analyses of that problem in the literature. Most authors seem interested in the effect of a stabilizing temperature gradient on the shear instability and the case of an unstable stratification is seldom treated.

We numerically solved (4.10) for the special case of a Couette flow $\tilde{u}_0 = z$. A Couette flow has the special property of being linearly stable at all values of Re. It also probably corresponds more closely to the experimental situation. With a Couette flow additional symmetries arise in the problem (4.10) and one can set $c_{\mathrm{r}} = \frac{1}{2}$. Owing to those symmetries one can look for solutions such that $\theta_{\mathrm{r}}(z) =$

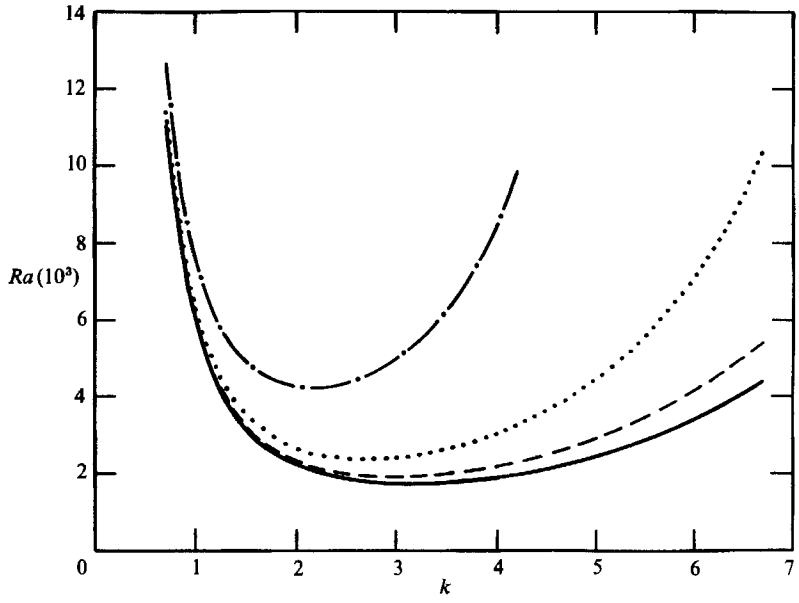

FIGURE 16. The marginal stability curve for convection with a shearing flow. The Prandtl number is 0.7. In ascending order the curves correspond to Reynolds numbers 0 (——), 20 (– – –), 40 (····) and 80 (—·—). The curves are the lower boundary of the stable regions.

$-\theta_r(1-z), \theta_i(z) = \theta_i(1-z)$, where $\theta = \theta_r + i\theta_i$. The solutions were found using a well-known technique (used for instance by Krueger, Gross & Di Prima 1966). First note that $z = \frac{1}{2}$ the symmetries of the equations allow a symmetric solution that verifies $\theta_r = D^2\theta_r = D^4\theta_r = 0$ and $D\theta_i = D^3\theta_i = D^5\theta_i = 0$. At $Re = 0$ the first mode that becomes unstable has these symmetries. There remain six unknown derivatives at $z = \frac{1}{2}$. To solve the problem we construct six linearly independent solutions $\theta^{(i)}$ in the following way: for $\theta^{(1)}$, $D\theta_r^{(1)}(\frac{1}{2}) = 1$ and all the other derivatives are 0. For $\theta^{(2)}$, $D\theta_r^{(2)}(\frac{1}{2}) = 0$, $D^3\theta_r^{(2)} = 1$, $D^5\theta_r^{(2)} = 0$ and all other derivatives zero. The four other solutions are similarly constructed. We then integrate from $z = \frac{1}{2}$ to $z = 1$. Using the boundary conditions (4.11) we obtain a matrix $A_{ij} = A_j[\theta^{(i)}(1)]$. A combination satisfying all the boundary conditions can be found if the determinant of A_{ij} is zero. Starting from $Re = 0$, $Ra = 1708$ and $k = 3.11$ we tracked the values of Ra and k for which the determinant first changed sign. The marginal stability curves of figure 16 show the effect of the shear, which is most pronounced at high values of k. We investigated only the range $1708 < Ra < 10^5$ since only a moderate increase in the boundary layer Rayleigh number is necessary to account for the experimental result. Indeed, one can notice that

$$Nu = \left(\frac{Ra}{Ra^{bl}}\right)^{\frac{1}{3}},$$

and hence from (2.1)

$$Ra^{bl}|_{Ra=10^{14}} = 10Ra^{bl}|_{Ra=10^7}.$$

If one assumes that at the transition from soft to hard turbulence Ra^{bl} has a critical value around 10^3, critical numbers Ra_c of order 10^4 are required.

The results thus obtained are summarized in figure 17 where we plot the minimum Ra required for instability versus $PrRe^2$. The two parameter values $Pr = 0.7$ and

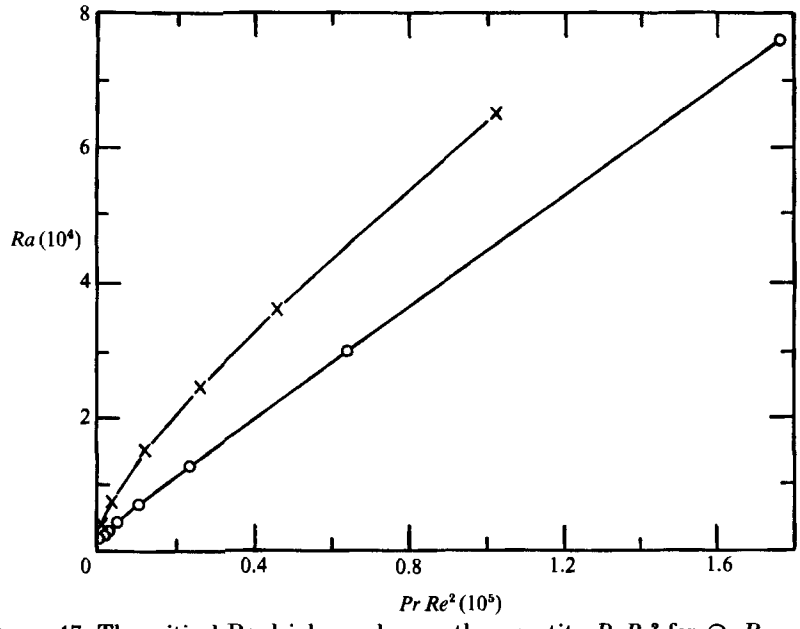

FIGURE 17. The critical Rayleigh number *vs.* the quantity $Pr\,Re^2$ for ○, $Pr = 0.7$ and ×, $Pr = 7$. Lines have been added to guide the eye. The data, however, are the points.

$Pr = 7.0$ were investigated. Results similar to those known for the Poiseuille flow were obtained. Our numerical results can be conveniently summarized by the relation

$$Ra_c^{bl} = A(Pr) + J_* Pr\,Re^2, \tag{4.13}$$

where $A(Pr)$ is independent of Re and the number J_* is analogous to a critical value of the Richardson number $J = (\alpha g \Delta\lambda)/u_0^2$. We found $J_* \approx 0.4177$ for $Pr = 0.7$ and $J_* \approx 0.5318$ for $Pr = 7.0$. However, we have been unable to support the conjecture (4.13) through some sort of asymptotic analysis. The attraction of this formula, however, is that the viscosity and thermal diffusivities do not occur in it. It is moreover well established through numerical analysis. At high values of Re, the stability of the boundary layer thus requires winds of order u_0 such that

$$u_0^2 \propto \alpha g \Delta\lambda.$$

From (3.11) and (3.17) one may get

$$\Delta\lambda = \Delta_m d_m,$$

and hence

$$u_0 \propto (\alpha g \Delta_m d_m)^{\frac{1}{2}}. \tag{4.14}$$

It is easy to object that rolls with axes parallel to the shearing wind will not be stabilized by this mechanism. However as the direction of the wind fluctuates it will stabilize rolls tending to grow in any direction. One might also want to know the origin of the wind u_0. This can clearly not be the wind of the central region. This wind blows in a steady direction over a long time, if not permanently. But it is possible to argue that the shearing wind is created in the mixing layer, or is due to a secondary flow on top of the central region wind. The velocity of the fluid below the gravity waves conjectured in §3.4 is precisely (4.14) since

$$u_0 \sim d_m \omega_p. \tag{4.15}$$

5. Conclusion

The experiment described here shows rather conclusively that there is a wide range of Rayleigh numbers for which helium obeys a set of simple scaling laws. The heuristic similarity analysis offers a possible explanation for this observed behaviour.

The major successes of the theoretical approach outlined here are:

(i) An acceptable prediction of the scaling indices β, γ, δ and ϵ.

(ii) The right general form for the temperature histogram in the hard turbulence region.

Weaknesses include:

(i) Poor predictive power for the actual geometry of layers and thermals.

(ii) The argument for the origin of ω_p is not completely convincing.

(iii) Less than compelling results for the Prandtl number dependence.

(iv) The stability argument for the boundary layer is new, but it is hard to assess the validity of the linearization used to derive it.

Clearly, our work here is a beginning not an end. The next steps should try to remedy the weaknesses mentioned above and also include:

(i) A careful study, including visualizations, of the flow patterns to ascertain the real geometries of the flow. We have said very little about the large-scale circulation, although preliminary experimental evidence suggests its importance.

(ii) An extension of this study to lower Rayleigh numbers or higher Prandtl numbers to obtain an understanding of how soft turbulence differs from hard turbulence.

(iii) A study of the fine structures of the turbulent motion. This entire paper has been focused on the gross patterns of the flow. We have seen that the cell gives a simple and controllable turbulent behaviour. One major goal of the next studies should be to look into the details of the turbulence observed here. More detailed knowledge of both space and time correlations should be sought. Velocities should be measured to supplement the temperature studied here.

(iv) Finally it would be very interesting to extend the experimental results and the theoretical concepts described here to higher values of the Rayleigh number. Many of the people we have discussed this work with believe that at higher Ra there will be a new and quite different behaviour. For instance Kraichnan (1962) predicts a new behaviour appearing between $Ra = 10^{18}$ and $Ra = 10^{24}$. We do not know. Perhaps the hard turbulence extends to infinitely high values of Ra, perhaps not.

We believe we have, following previous workers, devised an approach which can be very useful in getting at the core of one kind of turbulent motion. We must await future work to see whether this promise can be fulfilled through a gain in fundamental knowledge about the turbulent state.

We wish to thank Uriel Frisch, Philip Homsey, Robert Kraichnan, Willem Malkus, Alan Newell, Yves Pomeau, Ed Spiegel and Boris Shraiman for several fruitful conversations. We thank Anton Kast for helping with the data analysis. This work was supported in part by the University of Chicago Materials Research Laboratory. S.Z. was supported under NSF grant DMS-8603752 and by a NATO grant for international travel nr 85/0509 and wishes to thank the Department of Mathematics of MIT for its hospitality. B.C. was supported by a NATO grant.

REFERENCES

ANDERSON, A. C. 1973 Low-noise ac bridge for resistance thermometry at low temperatures. *Rev. Sci. Instrum.* **44**, 1475–1477.

BEHRINGER, R. P. 1985 Rayleigh–Bénard convection and turbulence in liquid helium. *Rev. Mod. Phys.* **57**, 657–687.

BRUNT, D. 1927 The period of simple vertical oscillations in the atmosphere. *Q. J. R. Met. Soc.* **53**, 30–32.

BUSSE, F. H. 1969 On Howard's upper bound for heat transport by turbulent convection. *J. Fluid Mech.* **37**, 457–477.

BUSSE, F. H. 1978*a* Non-linear properties of thermal convection. *Rep. Prog. Phys.* **41**, 1929–1967.

BUSSE, F. H. 1978*b* The optimum theory of turbulence. *Adv. Appl. Mech.* **18**, 77–121.

CHAN, S.-K. 1971 Infinite Prandtl number turbulent convection. *Stud. Appl. Math.* **1**, 13–49.

CHANDRASEKHAR, S. 1961 *Hydrodynamic and Hydromagnetic Stability*. Clarendon.

CHU, T. Y. & GOLDSTEIN, R. J. 1973 Turbulent convection in a horizontal layer of water. *J. Fluid Mech.* **60**, 141–159.

DATTA, S. K. 1965 Stability of spiral flow between concentric circular cylinders at low axial Reynolds number. *J. Fluid Mech.* **21**, 635–640.

DEARDORFF, J. W. & WILLIS, G. E. 1965 The effect of two dimensionality upon the suppression of thermal turbulence. *J. Fluid Mech.* **23**, 337–353.

ECKMANN, J.-P. 1981 Roads to turbulence in dissipative dynamical systems. *Rev. Mod. Phys.* **53**, 643–654.

FITZJARRALD, D. E. 1976 An experimental study of turbulent convection in air. *J. Fluid Mech.* **73**, 693–719.

FOSTER, T. J. & WALLER, S. 1985 Experiments on convection at very high Rayleigh numbers. *Phys. Fluids* **28**, 455.

GAGE, K. S. & REID, W. H. 1968 The stability of thermally stratified plane Poiseuille flow. *J. Fluid Mech.* **33**, 21–32.

GARRON, A. M. & GOLDSTEIN, R. J. 1973 Velocity and heat transfer measurements in thermal convection. *Phys. Fluids* **16**, 1818–1825.

GOLDSTEIN, R. J. & CHU, T. Y. 1971 Turbulent convection in a horizontal layer of air. *Prog. Heat Mass Transfer* **2**, 55–75.

GOLDSTEIN, R. J. & TOKUDA, S. 1980 Heat transfer by thermal convection at high Rayleigh numbers. *Intl J. Heat Mass Transfer* **23**, 738–740.

GOUGH, D. O., SPIEGEL, E. A. & TOOMRE, J. 1975 Modal equations for cellular convection. *J. Fluid Mech.* **68**, 695–719.

HERRING, J. R. 1963 Investigation of problems in thermal convection. *J. Atmos. Sci.* **20**, 325–338.

HERRING, J. R. 1964 Investigation of problems in thermal convection : rigid boundaries. *J. Atmos. Sci.* **21**, 277–290.

HESLOT, F. CASTAING, B. & LIBCHABER, A. 1987 Transition to turbulence in helium gas. *Phys. Rev.* A **36**, 5870–5873.

HOWARD, L. N. 1963 Heat transport by turbulent convection. *J. Fluid Mech.* **17**, 405–432.

HOWARD, L. N. 1966 Convection at high Rayleigh number. *Applied Mechanics, Proc. of the 11th Congr. of Appl. Mech. Munich (Germany)* (ed. H. Görtler), pp. 1109–1115. Springer.

HUGHES, T. H. & REID, W. H. 1967 The stability of spiral flow between rotating cylinders. *Phil. Trans. R. Soc. Lond.* A **263**, 57–91.

INGERSOLL, A. P. 1966 Thermal convection with shear at high Rayleigh number. *J. Fluid Mech.* **25**, 209–228.

KOSCHMIEDER, E. L. 1974 Bénard convection. *Adv. Chem. Phys.* **26**, 177–212.

KRAICHNAN, R. H. 1962 Turbulent thermal convection at arbitrary Prandtl number. *Phys. Fluids* **5**, 1374–1389.

KRISHNAMURTI, R. & HOWARD, L. N. 1981 Large scale flow generation in turbulent convection. *Proc. Natl Acad. Sci.* **78**, 1981–1985.

KRUEGER, E. R., GROSS, A. & DI PRIMA, R. C. 1966 On the relative importance of Taylor-vortex and non-axisymmetric modes in flow between rotating cylinders. *J. Fluid Mech.* **24**, 521–538.

LIBCHABER, A. & MAURER, J. 1982 A Rayleigh Bénard experiment: Helium in a small box. *Nonlinear Phenomena at Phase Transitions and Instabilities, Proceedings NATO ASI, Geilo Mar 29–Apr 9, 1981* (ed. T. Riste), pp. 259–286. Plenum.

LONG, R. R. 1975 Some properties of turbulent convection with shear. *Geophys. Fluid Dyn.* **6**, 337–350.

LONG, R. R. 1976 Relation between Nusselt number and Rayleigh number in turbulent thermal convection. *J. Fluid Mech.* **73**, 445–451.

LORENZ, E. N. 1963 Deterministic nonperiodic flow. *J. Atmos. Sci.* **20**, 130–141.

MCCARTHY, P. D. 1973 Thermophysical properties of He from 2 to 1500 K with pressure to 1000 Atm. *J. Phys. Chem. Ref. Data* **2**, 923–1024.

MALKUS, W. V. R. 1954*a* Discrete transitions in turbulent convection. *Proc. R. Soc. Lond.* A **225**, 185–195.

MALKUS, W. V. R. 1954*b* The heat transport and spectrum of thermal turbulence. *Proc. R. Soc. Lond.* A **225**, 196–212.

MALKUS, W. V. R. 1963 Outline of a theory of turbulent convection. In *Theory and Fundamental Research in Heat Transfer*. Pergamon.

MALKUS, W. V. R. & VERONIS, G. 1958 Finite amplitude cellular convection. *J. Fluid Mech.* **4**, 225–260.

MONIN, A. S. & OBUKHOV, A. M. 1953 Dimensionless characteristics of turbulence in the atmospheric surface layer. *Dokl. Akad. Nauk USSR* **93**, 257–260.

MONIN, A. S. & OBUKHOV, A. M. 1954 Basic turbulent mixing laws in the atmospheric surface layer. *Trudy Geofiz. Inst. Akad. Nauk USSR* no. 24 **151**, 163–187.

MONIN, A. S. & YAGLOM, A. M. 1971 *Statistical Fluid Mechanics, vol. 1*. The MIT Press.

PELLEW, A. & SOUTHWELL, R. V. 1940 On maintained convective motion in a fluid heated from below. *Proc. R. Soc. Lond.* A **176**, 312–343.

PRANDTL, L. 1932 Meteorologische Anwendungen der Strömungslehre. *Beitr. Z. Phys. Atmos.* **19**, 188–202.

PRIESTLEY, C. H. B. 1954 Convection from a large horizontal surface. *Austral. J. Phys.* **7**, 176–201.

PRIESTLEY, C. H. B. 1959 *Turbulent Transfer in the Lower Atmosphere*. The University of Chicago Press.

REID, W. H. & HARRIS, D. L. 1958 Some further results on the Bénard problem. *Phys. Fluids* **1**, 102–110.

ROBERTS, P. H. 1966 On non-linear Bénard convection. *Non-Equilibrium Thermodynamics, Variational Techniques and Stability. Proc. Symp. University of Chicago, May 17–19, 1965* (ed. R. J. Donnelly, R. Herman & I. Prigogine), pp. 125–127. The University of Chicago Press.

SPIEGEL, E. A. 1962 On the Malkus theory of turbulence. *Mécanique de la turbulence, Colloque Internationaux de CNRS a Marseille*, pp. 181–201. Éditions CNRS.

SPIEGEL, E. & ZALESKI, S. 1984 Shear induced instability in reaction diffusion systems. *Phys. Lett.* **106** A, 335–338.

TANAKA, H. & MIYATA, H. 1980 Turbulent natural convection in a horizontal water layer heated from below. *Intl J. Heat Mass Transfer* **23**, 1273–1281.

THRELFALL, D. C. 1975 Free convection in low-temperature gaseous helium. *J. Fluid Mech.* **67**, 17–28.

TOOMRE, J., GOUGH, D. O. & SPIEGEL, E. A. 1977 Numerical solutions of single mode convection equations. *J. Fluid Mech.* **79**, 1–31.

TOOMRE, J., GOUGH, D. O. & SPIEGEL, E. A. 1982 Time dependent solutions of multimode convection equations. *J. Fluid Mech.* **125**, 99–122.

TOWNSEND, A. A. 1959 Temperature fluctuations over an heated surface. *Fluid Mech.* **5**, 209–241.

TURNER, J. S. 1969 Buoyant plumes and thermals. *Ann. Rev. Fluid Mech.* **1**, 29–44.

VÄISÄLÄ 1925 *Soc. Fennica, Commun. Phys. Maths* **2**, 38.